Synthesis of in-silico designed plasmepsin X inhibitors and evaluation of their anti-plasmodial effects

Prem Prakash Sharma,[1,2] Monika Kumari,[1,2] Ravindra Kumar,[3]* Geeta Singh[1]*
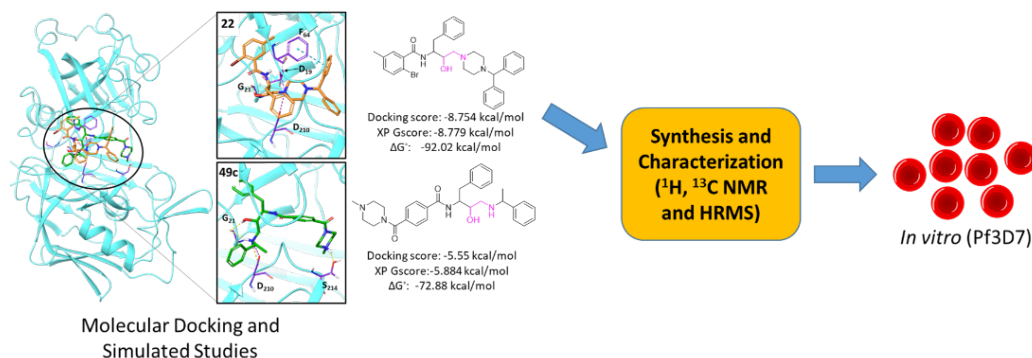
[1]Department of Biomedical Engineering, Deenbandhu Chhotu Ram, University of Science & Technology, Murthal, Sonepat Haryana 131039 India. [2]Laboratory for Translational Chemistry and Drug Discovery, Department of Chemistry, Hansraj College, University of Delhi, Delhi-110007 India. [3]Department of Botany, Hindu College, University of Delhi, Delhi-110007 India.

ABSTRACT

Molecular Docking and Simulated Studies

Plasmepsin X (*Pf*Plm X) protein plays a significant role in egression and invasion of malarial parasite *Plasmodium falciparum* (*Pf*) and is considered a promising target. All hydroxyethylamine (HEA) and piperazine based 313 analogs were screened against *Pf*Plm X protein. In computational study, compound **22** was identified as the most promising molecule which showed better docking results compared to **49c**. Compound **22** showed docking scores, XP Gscore, and ΔG˚ of −8.754 kcal/mol, −8.779 kcal/mol, and −92.02 kcal/mol, respectively while **49c** showed docking score, XP Gscore, and ΔG˚ of -5.550 kcal/mol, -5.558 kcal/mol, and -72.88 kcal/mol, respectively. An extensive MD simulation of 200ns also supported the docking results of compound **22**. Assayed for the initial screening against *Pf* Chloroquine (CQ)-resistant (INDO) culture suggested that compound **22** is a hit molecule with an inhibitory concentration of 6.8 μM. Next, compound **22** was also assessed for toxicity against liver cells, HepG2, and none of the two compounds showed cytotoxicity up to 100 μM. Overall, compound **22** demonstrated moderate anti-plasmodial activity without any toxic effects, and therefore medicinal chemistry optimization is essential to obtain analogs with improved inhibitory activity.

Keywords: Plasmepsin X, Hydroxyethylamine, Piperazine, Plasmodium falciparum, Molecular docking and simulation

INTRODUCTION

Despite the passage of several decades, malaria remains a terrible illness because of its pathogenicity and increasing resistance. *Plasmodium falciparum* (*Pf*), a member of the *Plasmodium* species, is the most virulent strain. Resistance development against current antimalarials causes a panic scenario, increasing the impact of malaria on human health and the economy. Consequently, malaria was still responsible for 241 million cases in 2020 alone, with an estimated 267,000 deaths worldwide.[1] Malaria management strategies include the use of bed nets, insect-repellent sprays, medications, and vaccinations[2,3] but there is still no prompt and effective malarial treatment. As a

result, there is an urgent need for novel malarial treatment options.

The RTS, S malaria vaccine was recently approved for use in *Pf* endemic regions, but its protective efficiency (36%) was low, requiring frequent boosters.[4] In the absence of effective vaccines, artemisinin-based combination therapies (ACTs) are the only viable options.[5] The molecular mechanism of conventional antimalarial treatments is still unknown.[2] Drug-resistant mutations arise during the parasite's sexual stages.[6] Antimalarial drug resistance in *Pf* strains is a worldwide health problem.[7] To effectively treat *Pf* infections and overcome resistance, two or more medications with various mechanisms of action are used nowadays. An increase of ACT-resistant strains from Southeast Asia, Eastern India, and Central Africa, as well as their inevitable spread to other places, pose serious difficulties to malaria eradication efforts.[8-12] It necessitates the discovery of more effective antimalarials.

During the intra-erythrocytic stage of infection, *Pf* digests the host cell Hb, which is required for the parasite's development. Plasmodium aspartic proteases termed plasmepsin/s (Plm/s),

*Corresponding Author: Dr. Geeta Singh & Dr. Ravindra Kumar
Tel: 0130- 2484201
Email: geetasingh.bme@dcrustm.org & ravijnu@gmail.com

digest host hemoglobin inside digestive vacuoles [13]. The Plm has ten distinct forms of which Plm I, Plm II, Plm IV, and histo-aspartic protease (HAP) belong to the food vacuole of *P. falciparum*. Plm V, which is found in the endoplasmic reticulum of *Pf*, is involved in the cleavage of proteins that are intended for Plasmodium export element (PEXEL) protein export into the host cell.[14] Plm IX and Plm X are expressed in late schizonts of the parasite's life cycle.[15] The rest of the plasmepsins VI-VIII belong to the exo-erythrocytic stage.[13] Most studies were done to target digestive food vacuole *Pf*Plm due to the availability of crystal structures in the protein database (www.rcsb.org). The serine protease subtilisin-like 1 (SUB1) has a significant role in the egression and invasion of malarial parasites where Plm X is required for the activation of a SUB1.[15] Ciana and co-workers observed that **49c** inhibits *Pf* NF54 strain on longer exposure (72h, IC$_{50}$ 0.6 nM) while modest inhibition effects were seen on 24h exposure with IC$_{50}$ >500nM (Ciana et al. 2013).[16] The chemical **49c**, which has a hydroxyethylamine (HEA) scaffold, was shown to be efficient against *Pf* (*in-vivo*).[17] In this study, we targeted *Pf*Plm X and virtually screened novel HEA and piperazine based analogs to find any potential inhibitor, synthesized potential compound and validated by biological assay. Homology model technique was used to predict the structure of *Pf*Plm X due to the unavailability of crystal structure. Then, docking and virtual screening studies were conducted to discover potential *Pf*Plm X inhibitors. The stability of the proposed inhibitor in a complex with Plm X was assessed through molecular dynamics simulation.

RESULTS AND DISCUSSION

Targeting of *Pf*Plm X has significant effects on parasite survival as hemoglobin degradation is very essential for their survival.[13,18] Designed analogs may inhibit *Pf*Plm X activity leading to parasite growth inhibition. This finding encouraged us to design and screen analogs against *Pf*Plm X using computational approaches.

2.1. Homology modeling of Plm X and structure validation

Due to the absence of Plm X structure, homology modeling was used to predict the Plm X structure. The cathepsin D (PDB: 5UX4) was used as a template to generate the model structure of *Pf*Plm X. There was sequence identity, sequence similarity, and sequence coverage of 33.66%, 98%, and 96%, respectively. Further, protein structure quality was analyzed by online tools such as ERRAT, Verify 3D, PROSA, and PROCHECK.[19]

The ERRAT plot (**Figure S1a**) showed a quality factor score of 81.44, and the Verify3D plot (**Figure S1b**) with 83.44% of residues showed averaged 3D-1D score >= 0.2. Quality assessment through the ProSA web server (**Figure S1c**) indicated that the modeled structure had a Z-score of -7.81. The generated model revealed strong stereo-chemical geometry of the residues as analyzed by the Ramachandran map, which is shown in **Figure S1d.** The modeled structure has only 3 outlier residues (Glu204, Gln238, and Asp271). There were 87.7%, 11.2%, and 0.4% residues in the favoured region, additional allowed region, and generously allowed region, respectively.

2.2. Molecular docking studies

Molecular docking calculations were performed to search for the HEA-piperazine analogs that can bind strongly within the active site of the *Pf*Plm X enzyme using GLIDE module. Glide was selected over other docking programs because it outperforms in achieving lower RMS deviations from native co-crystallized structures and finds the correct binding modes for a large set of test cases.[20] Docking score (kcal/mol) and glide XP Gscore (kcal/mol) were considered to rank the poses of the ligands depending on their computed binding affinity. In the case of *Pf*Plm X, all the 313 molecules docked within the binding pocket of *Pf*Plm X. We selected our top compounds based on the cut-off docking score (-8.0 kcal/mol), and XP Gscore (-8.0 kcal/mol) whereas **49c** showed docking score, and XP Gscore of -5.550 kcal/mol and -5.558 kcal/mol, respectively (**Figure 1b** and Table 1, entry 2). Therefore, we had a total of 18 out of 313 compounds having scores better than the cut-off docking score (Table 1, entry 1 and Table S1, entry 1-17). Molecules having docking scores lower than -8.0 kcal/mol can be seen in Table S2. Top-ranked compound **22** showed docking scores, XP Gscore, and binding free energy (ΔG˚) of –8.754 kcal/mol, –8.779 kcal/mol, and –92.02 kcal/mol, respectively (**Figure 1a** and Table 1, entry 1). The ΔG˚ of **49c** (-72.88 kcal/mol) was also lower than top-ranked compound **22** (-92.02 kcal/mol). There was no penalty for polar atom burial and desolvation penalties, no solvent expose penalties and, no epikstate penalties, compound **22** in complex with *Pf*Plm X (Table 1, entry 1). The rotatable penalty for compound **22** was 0.2 whereas **49c** possesses both epikstate penalty and rotatable penalty of 0.3 (Table 1, entry 1-2). The LipophilicEvdW rewards, H-bond rewards, and electrostatic rewards for compound **22** were -4.8, -2.2, and -2.2, respectively. On the other hand, **49c** showed lipophilicEvdW rewards, H-bond rewards, and electrostatic rewards of -3.7, -1.6, and -0.9, respectively. Due to these penalties and rewards, compound **22** showed a better docking score than **49c**.
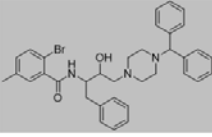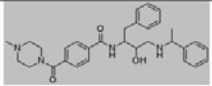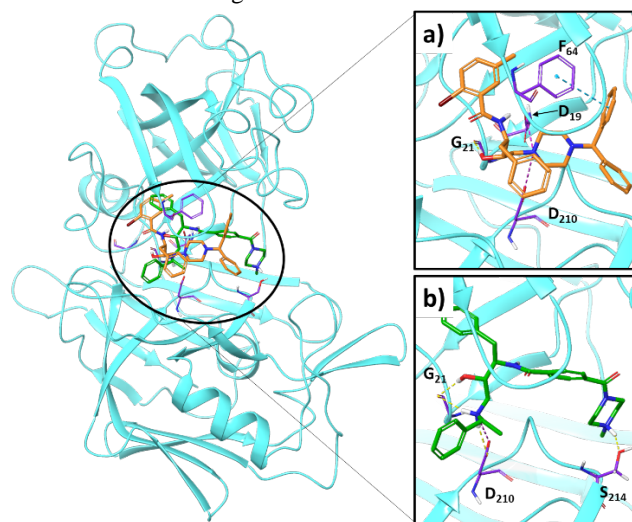

Figure 1. 3D- interaction diagram displaying ligand interaction in binding site; **a)** *Pf*Plm X-**22** complex, **b)** *Pf*Plm X-**49c** complex

Table 1. List of HEA-based hit molecules based on docking score (kcal/mol), XP Gscore (kcal/mol) and ΔG$^{\square}$ (kcal/mol) towards the targeted *Pf*Plm X protein

Entry no.	Compound code	Structures	Docking Score	XP Gscore	MMGBSA (ΔG)	Penalty	Solvent expose penalty	Epik state penalty	Rotatable bond penalty
1	22		-8.754	-8.779	-92.02	0	0	0	0.2
2	49c		-5.550	-5.884	-72.88	0	0	0.3	0.3

The 2D-interaction plots of the docked candidates of *Pf*Plm X protein are depicted in **Figure 2**. In the case of the *Pf*Plm X-**22** complex,1-benzhydryl substituted at pocket 2 interacted with Phe64 by pi-pi interaction (**Figure 2a**). Both catalytic residues (Asp19 and Asp210) interacted with the nitrogen atom of piperazine by salt bridge interaction while Gly21 interacted with a hydroxyl group of HEA by H-bond where Gly21 acted as a hydrogen bond acceptor (HBA).
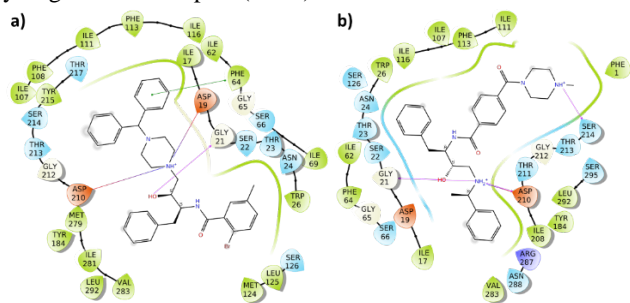

Figure 2. 2D- ligand interaction diagram showing ligand interaction to binding site residues; **a)** *Pf*Plm X-**22** complex, **b)** *Pf*Plm X-**49c** complex

In *Pf*Plm X-**49c** complex, Asp210 and Gly21 (HBA) interacted with the nitrogen atom of 1-phenylethanamine of **49c** by H-bond. Residue Asp210 also interacted with the nitrogen atom of 1-phenylethanamine by a salt bridge. The residue Ser214 acting as HBA interacted with the nitrogen atom of piperazine by H-bond (**Figure 2b**). Both ligands, compound **22** and **49c** in complex with *Pf*Plm X showed interaction with the same residues Asp210, and Gly21. Both complexes along with apo *Pf*Plm X were taken forward for MD simulation of 200ns to analyze the conformational stability of docked ligand.

2.3. Molecular dynamics simulations

Extensive molecular dynamics simulations were carried out for the period of 200ns to study the stability, and the conformational behaviour of compound **22** in complex with *Pf*Plm X and the results were compared with **49c** and apo *Pf*Plm X. The stability of these systems was measured by the root mean square deviation (RMSD) and root mean square fluctuation (RMSF) change for protein-ligand complexes during the

simulations. The RMSD plot of Cα-*Pf*Plm X in complex with compound **22**, **49c,** and unligated *Pf*Plm X attained stability within first 25ns and fluctuations were in acceptable region (≤3Å) (**Figure 3a-c**). The average value of RMSD$_{Cα}$, RMSD$_{backbone}$, and RMSD$_{sidechain}$ for the *Pf*Plm X in complex with compound **22** was 3.61±0.31Å, 3.59±0.31Å, and 4.85±0.25Å was slightly lower than **49c** (4.23±0.22Å, 4.21±0.22Å, and 5.38±0.19Å), respectively. The average value of RMSD$_{Cα}$, RMSD$_{backbone}$, and RMSD$_{sidechain}$ for the unligated-*Pf*Plm X was 3.77±0.29 Å, 3.76±0.29 Å, and 4.60±0.24 Å, respectively. RMSD of Cα, backbone, and sidechain of *Pf*Plm X in all 3 complexes were similar and showed protein was very stable indicating that there was not any major conformational change in protein structures.
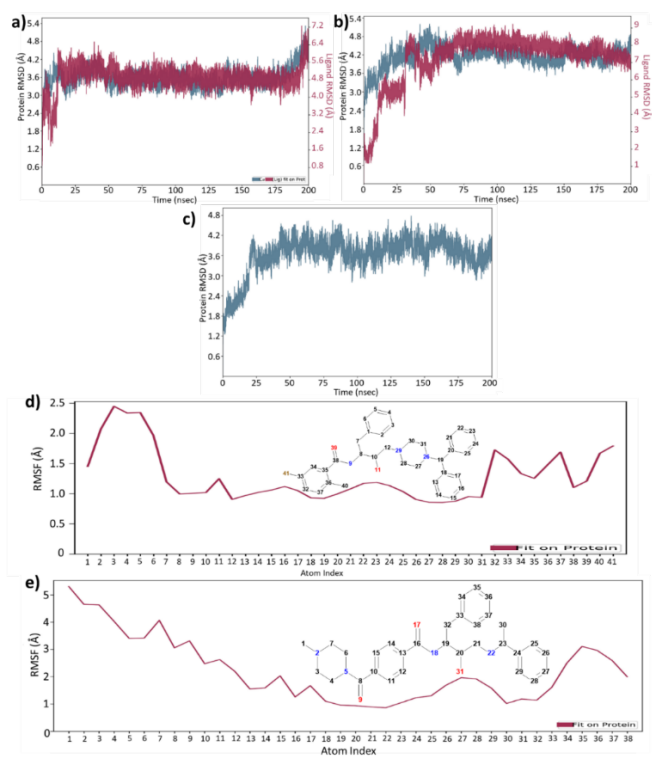

Figure 3. Cα-RMSD plot: **a)** *Pf*Plm X-**22** complex, **b)** *Pf*Plm X-**49c** complex, **c)** unligated-*Pf*Plm X complex; ligand-RMSF plot: **d)** *Pf*Plm X-**22** complex, **e)** *Pf*Plm X-**49c** complex

The average ligand RMSD$_{fit on protein}$ of compound **22** was 5.08±0.34Å which was significantly lower than **49c** (7.67±0.67Å) as depicted in **Figure 3a, b**. The RMSF plot indicated that most of the atoms of compound **22** fluctuated below 2Å while most of the atoms of 49c fluctuated more than 2Å (**Figure 3d, e**). Trajectory analysis revealed that the benzyl ring of HEA in compound **22** fluctuated most which was also supported by the RMSF plot.

In addition, the interactions between compound **22** and the binding site residues of *Pf*Plm X were studied (**Figure 4a**). It was observed that compound **22** showed similar conformational behavior and was able to maintain interactions with hotspot residues (Asp19, Phe64, and Asp210) which was also seen in molecular docking results. However, there were some other interactions with residues such as Ile11, Phe113, and Ile116.

Even **49c** interacted with Asp19, Phe64, Ile116, Tyr184, and Asp210 (**Figure 4b**). We observed that both ligands have some common residue interactions which suggested conformational stability of ligands.
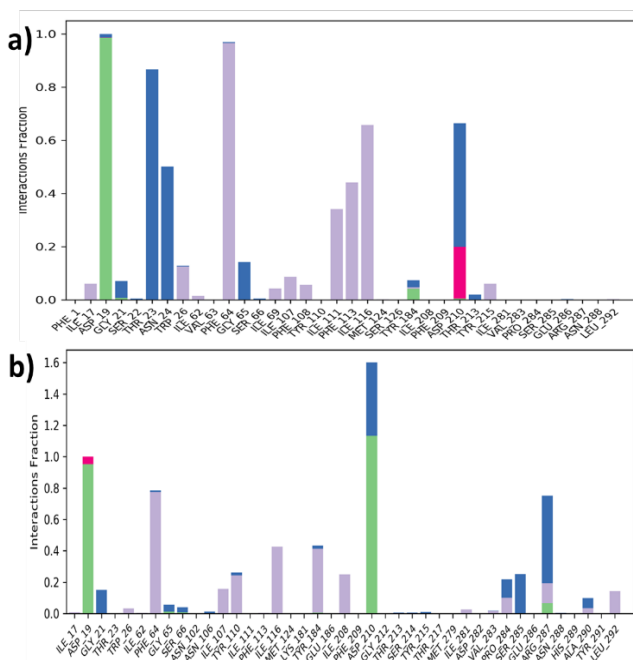

Figure 4. Ligand contacts histogram: **a)** *Pf*Plm X-**22** complex, **b)** *Pf*Plm X-**49c** complex; Interaction types: H-bond, Salt bridge, hydrophobic and water bridge.

Dynamic cross-correlation matrix (DCCM) analysis for PfPlm X

As seen in **Figure 5a-c**, compound **22** increased correlated movements, notably for residues near the binding site, compared to compound **49c**. The correlation change showed that the complex had more fluctuations and residue interactions than **49c**. There was also a disturbance of the original allosteric network between protein residues. **Figure 5** shows the correlation and anti-correlation of *Pf*PmX-**22** complex with *Pf*PmX-**49c**. Area A_1 represented more correlation among secondary structures β_{1-3} (**Figure 5a, b**). The loop β_4 and β_5 were less correlated with β_5 and β_6 as depicted in A_2 while more correlated with β_1 and β_2 shown in A_3.

There is a decrease in anti-correlation between β_{1-3} and the loop of β_{8-9} depicted in A_5. Also, there is a decrease in anti-correlation between β_{1-3} and β_{10-17} shown in A_7. The secondary structure β_{13-14} showed more correlation with β_{1-4}, and the loop of β_{4-5} as shown in A_8 and A_9, respectively. The α_2 and loop of α_2 and β_{17} are less anti-correlated with β_{1-2} as shown in A_{10} as well as a loop of α_2 and β_{17} less correlated with the loop of β_4 and β_5 as shown in A_{11}. Even β_{1-2} is more anti-correlated with β_{18-20} shown by A_{12}. The loop of α_2 and β_{17} as well as secondary structure β_{17} showed increased anti-correlation with α_1, β_{10}, and the loop of α_1 and β_{10} as depicted by A_{13}.

The Ramachandran plot of the last frame of 200ns simulation for both complexes and unligated-*Pf*Plm X showed residues lie ($\leq 1.1\%$) in the outlier region indicating good stereo-chemical geometry of the protein (**Figure S2** and Table S3; entry 1-3). The *Pf*Plm X-**22**, *Pf*Plm X-**49c**, and unligated-*Pf*Plm X possessed 3 (Glu203, Lys196, Asp271), 1 (Thr236), and 1 (Glu311) residues in the outlier region, respectively.

2.4.   Ligand Properties

Six properties as ligand RMSD (ligand fit over ligand), molecular surface area (MolSA), radius of gyration (rGyr), polar surface area (PSA), intramolecular H-bond (intraHB), and solvent accessible surface area (SASA) were analyzed to explain the stability of the compound **22** within *Pf*Plm X receptor binding pocket as shown in **Figure 6**. Compound **22** showed low ligand RMSD (ligand fit on ligand) compared to **49c** in complex with *Pf*Plm X (**Figure S3**). The radius of gyration was also lower for compound **22** compared to **49c**. Even other parameters were also better than **49c**.
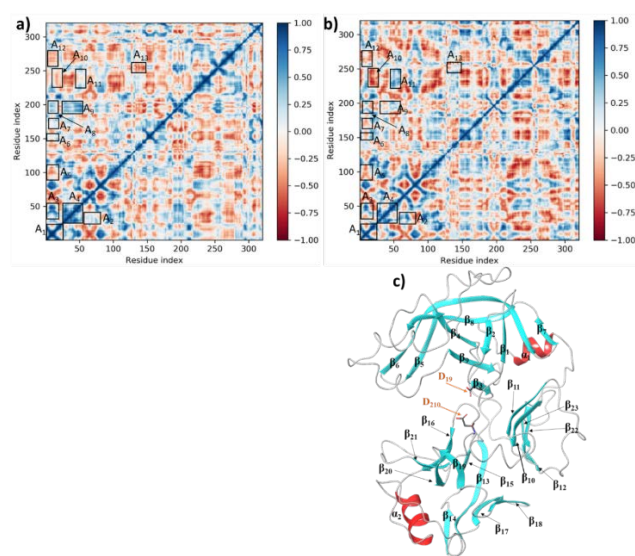

Figure 5. a) *Pf*Plm X-**22** DCCM plot, **b)** *Pf*Plm X-**49c** DCCM plot and **c)** labeled secondary structure of *Pf*Plm X
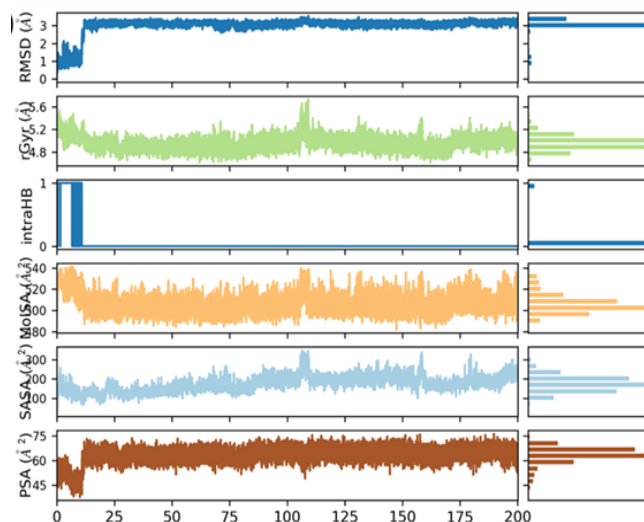

Figure 6. Ligand properties during the 200-ns simulations: *Pf*Plm X-**22** complex.

2.5. MMGBSA Free Energy Analysis

The MMGBSA calculations were used to quantitatively elucidate the energetics of compound **22** binding. The ΔG˚ was calculated at an interval of every 2ns for compounds **22** (16ns) and **49c** (60ns) after achieving the conformational stability in the complex with *Pf*Plm X (Table S4). As was shown by the MMGBSA analysis, the ΔG˚ for *Pf*Plm X-**22** complex was -107.89±9.33 kcal/mol, while for the *Pf*Plm X-**49c** complex, the result was –86.19±5.71 kcal/mol. A lower ΔG˚ for the *Pf*Plm X-**22** complex showed that compound **22** binding was more stable as compared to **49c**.

2.6. Docking Validation by non-site-specific docking

Non-site-specific docking indicated that compound **22** docked to the binding site of *Pf*Plm X only which means there was no allosteric site for our compound (**Figure 7**).
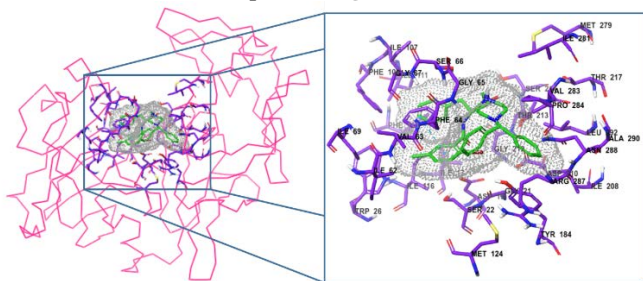

Figure 7. Docking validation by non-site-specific docking

2.7. ADME properties

The ADME profile through SwissADME was calculated for compound **22** where it obeyed Lipinski rule of five with H-bond donors (2), MLogP (<4.59), and H-bond acceptors (<4) except for the molecular weight of 612.6 g/mol (>500 g/mol). Compound **22** had TPSA score of 55.81 Å² and poor water-soluble nature. It has shown high GI tract absorption and possessed permeability to the blood-brain barrier. All of them have a nature of Pgp substrate as well as may inhibit all cytochromes (CYP1A2, CYP2D6, CYP2C19, and CYP3A4) except CYP2C9. Hence, compound **22** has drug-likeness property that is a matter of further validation by wet lab experiments.

2.8. Structure−Activity Landscape Index (SALI) Similarity Map Compounds Structure−Activity Landscape Index (SALI) Similarity Map Compounds in complex with *Pf*Plm X

Initially, the pocket-I having 2-bromo-5-methyl benzoic acid was kept constant and the substitutions were made at pocket-II which was linked to piperazine moiety. A total of 11 different compounds (**Figure S4**) were ranked on basis of docking scores with variations at pocket II; compound **22, 251, 165, 280, 51, 79, 107, 309, 136, 222,** and **194** (Table S5, entry 1–11). All 11 compounds containing different functional groups at pocket II such as benzhydryl, tert-butyl)benzyl, 4-(trifluoromethyl)benzyl, 3-(trifluoromethyl)benzyl, 4-methylbenzyl, 4-flourobenzyl, benzyl, 2-fluorobenzyl, 2,5-difluorobenzyl, phenyl, and 2-methylbenzyl were shown to possess higher docking scores in comparison to **49c** (-5.55 kcal/mol). During structure-activity

relationship (SAR) analysis of compounds in which pocket I was kept constant, two pairs of compounds, **165** and **280** having a similarity of 95% while **51** and **79** showed a structural similarity of 97% (as depicted in **Figure S4**). However, docking score was very close in compounds **165** (-7.211 kcal/mol) and **280** (-7.092 kcal/mol) as both molecules have –CF₃ group differing by *para* and *meta* position of benzyl ring of trifluoromethyl benzyl piperazine, respectively. It shows no significant effects of the isomeric (*ortho* and *para*) position of trifluoromethyl benzyl moiety on docking score. But when we compared compound **165** and **280** with compound **251**, there was a significant effect of the electron donating group (EDG) over the electron-withdrawing group (EWG) on docking score. The methyl group at *para* position in compound **51** showed a better docking score than compound **79** (-6.282 kcal/mol), **309** (-6.116 kcal/mol), and **136** (-6.006 kcal/mol) which contained EWG at *para*, *ortho*, and both ortho-meta position of benzylpiperazine, respectively. These EWG didn't show any significant effects on docking scores of **79**, **309**, and **136**. The methyl group at *para* position in compound **51** shows a docking score -6.997 kcal/mol while same methyl group at *ortho* position in compound **194** shows docking score -5.927 kcal/mol. This indicates that EDG at *para* position of benzylpiperazine has better effects on docking scores compared to *ortho* position. Compound **107** and **222** differ by benzyl and phenyl moiety at piperazine, which showed docking scores of -6.281 kcal/mol and -5.987 kcal/mol, respectively. There was no significant effect of benzyl group compared to phenyl ring on docking score. The docking score increased with increase in benzyl ring at pocket II as depicted by structure of compound **22**.

In the next attempt, variations were made at pocket-I while keeping the benzhydryl group constant at pocket-II then 27 distinct functionalities (**Figure S5**) were shortlisted **24, 2, 3, 14, 8, 17, 10, 19, 15, 20, 26, 7, 5, 21, 29, 25, 9, 16, 18, 6, 11, 23, 1, 4, 12, 13,** and **27** (Table S5, entry 12-38). But only compounds **2, 3, and 24** showed docking scores better than -8.0 kcal/mol. Similarly, SAR analysis of compounds having constant pocket II, showed seven groups of compounds having structural similarity of >95% such as compounds (**22**, **20**, and **18**), (**24**, and **13**), [**6**, **9**, and **11**), [**14** and **15**), (**10** and **1**), (**21** and **23**), and (**17**, **26**, **7**, **25**, and **12**).

The compound **22**, **18**, and **27** showed bromine (Br) atom at ortho position of benzoic acid while substitutions made at meta position showed significant effects on docking score. The fluorine (F) atom as strong EWG at meta position of benzoic acid in compound **18** showed docking score of -6.471 kcal/mol which decreased with substitution of less EWG at meta position as shown in compound **27** (-5.499 kcal/mol). The docking score increased with the substitution of EDG at meta position as in compound **22** (-8.754 kcal/mol). The strong EWG at para position of benzoic acid in compound **14** exhibited a better docking score than compound **15** as it has less EWG at para position. The carboxylic group at position meta (compound **4**) and para (compound **1**) show less docking score compared to carboxylic acid at ortho position in compound **3**. It indicated that carboxylic group at meta and para position had no significant effects compared to ortho position.

The comparison of para substituted benzyl alcohol in compound **10** showed a better docking score than compound **1** having a carboxylic group. Less EWG at both ortho positions of benzoic acid in compound **24** showed a better docking score than strong EWG at both ortho position of compound **13**. Compound **9** having EWG at para position showed a better docking score than compound **6** and **11** having EDG at para position. Compound **26** and **7** (both having methyl group at meta position) showed similar docking scores while bromine didn't show significant effects on the docking score of the compound **26**. There was slight decrease in docking score if we replace methyl group (compound **26**) with iodine (compound **25**). If we replace both halide groups (compound **25**, -6.838 kcal/mol) with 2 methyl groups (compound **12**, -5.788 kcal/mol) on both meta positions it showed a decrease in docking score. A significant change in docking score was observed if we replace one methyl (compound **12**, -5.788 kcal/mol) at meta position with bromine (compound **26**, -7.140 kcal/mol). Both compounds **21** and **23** possessed bromine atom at the para position but both compounds differ by fluorine and methyl group at ortho position, respectively. A significant increase in docking score was seen in compound **21** (-6.911 kcal/mol) having EWG at ortho position compared to compound **23** (-6.252 kcal/mol) having EDG in the same position.

The synthesis of novel HEA−piperazine analogs is depicted in Scheme 1. The synthetic procedure began with a simple, rapid, and regioselective ring opening of epoxide, (2R,3S)-3-(N-BOC-amino)-1-oxirane-4-phenylbutane (**I**) with 1-benzhydrylpiperazine (**II**) under microwave radiations that led to a Boc-protected intermediate (**III**) i.e., tert-butyl ((2S,3S)-4-(4-benzhydrylpiperazin-1-yl)-3-hydroxy-1-phenylbutan-2-yl)carbamate, which was then treated with trifluoroacetic acid (TFA) to obtain deprotected compound **IV** ((2S,3S)-3-amino-1-(4-benzhydrylpiperazin-1-yl)-4-phenylbutan-2-ol). Next, coupling of 2-bromo-5-methylbenzoic acid (**V**) with **IV** was accomplished to isolate the desired compound **22** (N-((2S,3S)-4-(4-benzhydrylpiperazin-1-yl)-3-hydroxy-1-phenylbutan-2-yl)-2-bromo-5-methylbenzamide) in 58% yield. Chemical structures of the newly synthesized compounds were characterized by NMR (1 H & 13C) and high-resolution mass spectrometry (**Figure S6−S8**).

2.9.   Biological Evaluation:

The effect of potent compounds **22** on the asynchronous *Pf* INDO growth inhibition in culture was evaluated using SYBR green assay in parasites. It was observed that the efficacy of compounds was studied at two different time points at 24hr and 48hr. There was a significant reduction in the parasite growth at 24hr having IC_{50} value of 6.8 µM (**22**). However, there was no noticeable reduction in IC_{50} at 48hr, suggesting the parasite killing occurs at 24hr affecting the first cycle of developmental stages. Compound **22** exhibited the highest efficacy with lesser IC_{50} values. These results indicate that compounds **22**, has immense therapeutic potential in treating clinical-resistant *P. falciparum*. Next, compound **22** was tested on HepG2 cells for their cytotoxicity evaluation and none of them found toxic upto 100 µM.

METHODS

3.1.   Homology modeling and structure validation

The Plm X structure was modeled using Swiss model tool (https://swissmodel.expasy.org/).[21] Cathepsin D of *Rattus norvegicus* (PDB: 5UX4) was taken as a template for Plm X structure modeling. The stereo-chemical geometry of Plm X residues was measured by the Ramachandran map (By Procheck).[22] The structural quality of modeled structure was analyzed by ERRAT, Verify3D, and PROSA.[23-25] The computational work was performed using Schrodinger software.

3.2.   Preparation of *Pf*Plm X and active site identification

The modeled structure was prepared to remove structural defects.[26] Strained bonds/angles as well as steric clashes were also rectified using energy minimization during protein preparation. Residues involved in the binding site were predicted through CastP server.[27] Protein model was refined by performing 20ns MD simulation before the docking studies.

3.3. Preparation of molecular library for virtual screening

The earlier reported **49c** (Zinc database ID:ZINC000218329015) inhibits *Pf*Plm X protein, and its structure file was obtained from zinc database.[28] In this present study, peptidomimetic, **49c** was considered as a control for *Pf*Plm X. A library of 313 molecules was developed based on HEA and piperazine pharmacophores by using the MAESTRO tool to target *Pf*Plm X (Table 4.1, entry 1, Table S1, entry 1-17, and Table S2, entry 1-295).[29] HEA-based compounds provide several benefits including fast, easy, big-scale synthesis and their potential against various diseases.[30-32] Before molecular docking, the structure of both **49c** and the library of HEA and piperazine-based analogs were prepared by Ligprep.[33] All parameters excluding chirality parameters for protease inhibitors and designed analogs were kept default. The chiralities were retained specified for both **49c** and designed analogs (SS conformer was specifically selected for HEA pharmacophore) (**Figure S9**). Desaltation for all ligands was done during tautomer generation. The inbuilt Epik module of the Schrodinger suite was used to estimate ionization states at pH 7 ± 2 for all compounds.[34] All ligands were screened against their respective protein.

3.4.   Molecular docking studies.

The site-specific docking of both **49c** and designed analogs against *Pf*Plm X was performed with the Glide module.[35] The parameters were kept default during grid generation by using Glide where van der Waals radii were scaling factor and partial charge cutoff as 1.0 and 0.25, respectively. The grid center coordinates for *Pf*Plm X were X= 20.697, Y = -14.274, Z = 25.319. The size of the cubical grid box was 30 Å. The molecular docking was performed at extra precision (XP). The ΔG˚ for **49c** and top-ranked compounds were also calculated by prime MMGBSA.[36]

3.5.   Molecular dynamics simulations

Molecular dynamics simulations of the selected docked complexes were performed to retrieve detailed insight into the dynamic behavior of the docked complexes along with the selected control. All the molecular dynamics simulations were conducted in the academic Maestro-Desmond tool with the in-built OPLS-2005 force field.[37-40] Before conducting simulations,

the docked complexes were solvated with the TIP3P water model in a $10×10×10$ Å^3 orthorhombic box.[41] The cation (Na$^+$) and anion (Cl$^-$) were added to neutralize the systems as well as to maintain the physiological pH. Before simulations, all the systems were energetically minimized for 100ps at default conditions. The Martyna–Tobias–Klein, and Nose–Hoover chain dynamic algorithm were used to maintain the pressure 1.0 bar and temperature of the systems at 300 K, respectively.[42,43]

Thereafter, the production run of 200ns time duration was carried out on both the prepared docked systems. The coordinates and energy were saved at 10.0ps and 1.2ps for *Pf*Plm X, respectively. Properties like RMSD, RMSF, protein-ligand interactions, and contacts were scrutinized to check the stability of the docked complexes. The stereo-chemical geometry of *Pf*Plm X was analyzed after MD simulation by Procheck.[22]

3.6. Validation of docking studies

Top-ranked compounds based on glide docking score and XP GScore in site-specific glide docking were further re-screened through non-site-specific blind docking using Autodock Vina in PyRx (version 0.8) [44]as a means of docking validation. In PyRx, the universal force field and the conjugate algorithm were used to minimize all compounds before blind dockings. The results were analyzed on the pymol platform (The PyMOL Molecular Graphics System).[45] The protein structure prepared in maestro was used in non-site-specific docking studies.

3.7. Absorption, distribution, metabolism, excretion, and Toxicity (ADMET) calculation

ADMET profiles of promising compounds were calculated by using Swiss ADME.[46] The predicted ADME properties include molecular weight (MW), rotatable bonds, HBA, HBD, TPSA (total polar surface area), predicted octanol/water partition coefficient (MLogP), solubility (ESOL class), GI absorption, BBB permeant, P-glycoprotein substrate, cytochrome inhibitor (CYP1A2, CYP2C19, CYP2C9, CYP2D6, and CYP3A4), Lipinski (drug-likeness).

3.8. General

Reagents and solvents used during the synthesis of desired compounds were purchased from commercial sources and used as it is without further purification. The progress of the reaction was monitored using thin layer chromatography (TLC) on alumina-coated plates (Merck). The purification of the compound was accomplished using flash chromatography (Yamazen, Japan) where alumina gel column with size of silica particles, 100-200 mesh was used. The initial step of compounds *i.e.* ring-opening reactions were performed under microwave conditions in a closed vial applying a closed dedicated microwave apparatus "Start Synth Microwave Synthesis Labstation (Milestone Microwave laboratory systems)" at optimized controlled temperature and time with a power supply of 300 W. Nuclear Magnetic Resonance (NMR) ^{1}H & ^{13}C spectra were obtained in CDCl$_3$ solvent media on a JEOL ECX-400P NMR spectrometer at 400 and 100 MHz respectively, at USIC, University of Delhi. Trimethylsilane (TMS) was taken as an internal standard for the analysis of NMR spectra of synthesized compounds. Melting points of final compounds were measured on a "BUCHI Labortechnik AG CH-9230" using open glass capillary tubes.

The molecular weight of the newly synthesized compounds was recorded at high-Resolution Biosystems Q-Star Elite-time-of-flight electrospray mass spectrometer.

General Procedure for Synthesis and Spectroscopic Data

To synthesize the hit compound there were three key steps to be followed, i) ring opening reaction of epoxide with piperazine derivatives; ii) protection of the Boc-group; and iii) coupling reaction with the acidic group. These steps were already well-explored in literature and our group has optimized each step for these types of compounds such as first and initial step was optimized under microwave irradiation[30], second step include the use of trifluoroacetic acid in dichloromethane followed by neutralization of reaction mixture using 1N NaOH[47]; and final step was carried out with the help of coupling reagents such as EDC.HCl, HOBt in dichloromethane at room temperature.[48,49] All these optimization reactions were followed to obtain the desired compounds and synthetic pathway of same is outlined in **Scheme 1**. The superficial regioselective ring opening of one of the most popular epoxide i.e., (2R, 3S)-3-(N-Boc-Amino)-1-oxirane-4-phenylbutane (**I**) with substituted 1-benzhydrylpiperazine (**II**) to afford compound (**III**) carried out under microwave conditions following the similar procedure as optimized by our research group.[30] A mixture of epoxide (**I**) (1.9 mmol) and 1-benzhydrylpiperazine (**II**) (1.9 mmol) and 5 mL of Ethanol were taken in a 50 mL round bottom flask, and the contents were heated under microwave-irradiation by controlled temperature programming upto 80°C. After completion of reaction, excess ethanol was evaporated under reduced pressure, and desired compound (**III**) i.e., tert-butyl ((2S,3S)-4-(4-benzhydrylpiperazin-1-yl)-3-hydroxy-1-phenylbutan-2-yl)carbamate was recrystallized using Hexane: Ethyl acetate (90:10). Next, the Boc-group of compound **III** was removed using excess of trifluoroacetic acid (15%) in dichloromethane at room temperature for 3-4 h. After completion, reaction mixture was neutralized using 1N NaOH and extracted with brine solution (15 mL x 3). The organic layer was dried over anhydrous sodium sulfate and evaporated under reduced pressure to afford intermediate (**IV**) as represented in **Scheme 1**.
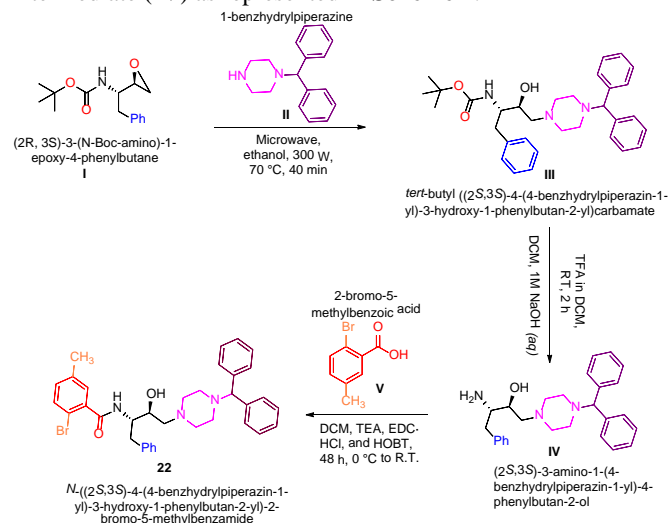
Scheme 1. Synthetic pathway of the hit compound **22** identified against *Pf*Plm X through extensive computational studies

The obtained intermediate was used as it is without further purification for its coupling with the respective aromatic acidic group (**V**) to obtained the final compound **22**. The coupling reaction was carried out as per already reported methods, which were adopted in previous research carried out by our group.[50,51] Initially, the aromatic acidic group (**V**) was dissolved in dichloromethane followed by the addition of trimethylamine (TEA, 3 eq.), and the reaction mixture was stirred for 20 min. at room temperature. Next, EDC.HCl (2 eq.) was added to the reaction mixture and was stirred for another 20 min followed by the addition of HOBt (2 eq.) and again stirred for another 20 min. Lastly, the obtained intermediates (**IV**) were added to the reaction mixture at ice-cold conditions, and the reaction mixture for stirred for 24 h at room temperature. After completion of the reaction, excess dichloromethane was evaporated under reduced pressure and the compound is extracted in ethyl acetate (20 mL x 3 times) and brine solution (15 mL x 3 times). The organic layer was dried over anhydrous sodium sulphate and excess solvent was evaporated under reduced pressure to afford the crude products as compound **22**. Further, the purification of compounds was carried out in Flash column chromatography using hexane and ethyl acetate as solvent system (70:30), which obtained compound **22** in 58%, yield.

N-((2S,3S)-4-(4-benzhydrylpiperazin-1-yl)-3-hydroxy-1-phenylbutan-2-yl)-2-bromo-5-methylbenzamide (22):

R_f value, 0.75 (9:1 chloroform/methanol); yield, 58%; mp, 126–129 °C; ^{1}H NMR (400 MHz, CDCl$_3$) δ 7.43 – 7.34 (m, 5H), 7.32 – 7.22 (m, 9H), 7.16 (dd, J = 15.3, 7.9 Hz, 2H), 7.03 (dd, J = 8.6, 6.3 Hz, 2H), 6.39 (d, J = 9.5 Hz, 1H), 4.34 – 4.23 (m, 1H), 4.19 (s, 1H), 3.78 (dd, J = 11.2, 2.9 Hz, 1H), 3.51 – 3.12 (m, 2H), 3.13 – 2.96 (m, 2H), 2.95 – 2.80 (m, 1H), 2.73 – 2.59 (m, 4H), 2.46 – 2.30 (m, 4H), 2.26 (d, J = 4.9 Hz, 3H). ^{13}C NMR (101 MHz, CDCl$_3$) δ 167.65 (s), 142.60 (s), 138.29 (s), 138.29 (s), 133.06 (s), 131.98 (s), 130.10 (s), 129.86 (s), 128.89 (s), 128.58 (s), 127.83 (s,), 127.09 (s), 126.59 (s), 115.67 (s), 65.32 (s), 60.39 (s), 52.54 (s), 52.01 (s), 38.97 (s), 20.85 (s). ESI (HR-MS) m/z (M+H) calcd for $C_{35}H_{38}BrN_3O_2$ 614.21269; found 614.20525.

3.10. In vitro anti-plasmodial activity against CQ-resistant *P. falciparum*:

Determination of blood stages and percent parasitemia was performed by Giemsa-stained thin smears from parasite cultures. Antimalarial inhibition activity (IC$_{50}$) was measured using the SYBR Green I assay[52], as reported asynchronous parasites from CQ-resistant (INDO) cultures were incubated in the presence of 1: 2 serial dilution of each compound tested for 24 and 48 h, in concentrations ranging from 25-0.78 µg/ml. Fluorescence intensity was determined using the BioTek Synergy HTX Multi-Mode Microplate Reader, with excitation and emission wavelengths of 485 and 530 nm, respectively, and analyzed by nonlinear regression with Normalization and Baseline corrections using software GraphPad Prism to determine IC$_{50}$ values.

3.11. Cytotoxicity effect of compound on HepG2 human cells

Cytotoxicity against human cell lines (HepG2) was determined using 3-(4,5-dimethylthiazol-2-yl)-2,5-diphenyltetrazolium bromide (MTT) dye. The MTT assay was performed in order to measure the cytotoxicity of the compound **22** on HepG2 cells.[48,49] HepG2 cells were maintained at 37°C, 5% CO$_2$ in sterile culture flasks and complete DMEM medium supplemented with 5% FBS, gentamicin (40 mg/ mL). Media was changed three times a week. The cells were trypsinized (0.05% trypsin/0.5 mM EDTA), washed and, distributed in 96-well plates (5000 cells/ well), followed by incubation for another 24 h at 37°C. The test compound **22** and DMSO were added in triplicate. After a 48-h incubation at 37 ºC, the supernatant was removed and 100 µL of MTT solution in complete DMEM was added to each well, followed by 2 h, incubation at 37 ºC. Undissolved precipitates were made solublised in DMSO and the culture plates were read in a spectrophotometer (Tecan infinite M200, nanoquant, UK) with a 490-nm filter. To determine cytotoxic concentrations a dose response curve was prepared.

CONCLUSION

The *Pf*Plm X is expressed in mature blood phase schizonts and invasive merozoites which enhances the pathogenicity of *Pf* parasite. The resistance development in *Pf* against ACT causes failure of current treatment approaches which necessitates for designing of novel molecules against known key target i.e., *Pf*Plm X. In our study, the 3D model of *Pf*Plm X was generated and validated. We screened a library of 313 compounds having HEA pharmacophore and piperazine. Finally, 18 compounds showed a better docking score than the cut-off value (-8.00 kcal/mol). The stability of top-ranked compound **22** in complex with *Pf*Plm X was further validated by 200ns MD simulation, post-MD analyses, and MMGBSA binding free energy calculation, and results were compared with known inhibitor **49c**. The docking result of compound **22** (-8.754, -8.779, and -92.02 kcal/mol) was far much better than that of compound **49c** (-5.550, -5.884, and -72.88 kcal/mol). The lower values of both RMSD, and RMSF of compound **22** as well as thermodynamic binding free energy analysis for every 2ns during MD simulation suggested compound **22** as potential inhibiting agent of *Pf*Plm X. Initially, the synthesis of identified analog (through extensive computational studies) was carried out with the earlier optimized methodology. The synthesis was confirmed via spectroscopic techniques such as 1H-NMR, 13C-NMR, and high-resolution mass spectroscopy (HRMS). Next, in order to validate the targets of compounds, biological evaluation was carried out. Our biological results indicated that compounds **22** showed immense therapeutic potential in treating clinical-resistant *Pf*. Further studies are needed to understand the mechanism of parasite killing and effect of the compound on other life stages of the parasite cycle. Experiments are in progress to observe their efficacy against the plasmepsins.

SUPPLEMENTARY INFORMATION

Quality of *Pf*Plm X model, Stereo-geometry of *Pf*Plm X, Ligand properties (RMSD, radius of gyration, intramolecular

hydrogen bond, MolSA, SASA, PSA), Docking results of other ligands, Spectral data (1H, 13C NMR, HRMS) of compound **22**, MMGBSA data, and Structure activity relationship for *Pf*Plm X.

CONFLICT OF INTEREST:

Authors declare no conflict of interest.

REFERENCES

1. WHO "World Malaria Report," **2021**.

2. E.G. Tse, M. Korsik, M.H. Todd. The past, present and future of anti-malarial medicines. *Malar. J.* **2019**, 18, 93.

3. C. Nsanzabana. Resistance to artemisinin combination therapies (ACTs): do not forget the partner drug! *Trop. Med. Infect. Dis.* **2019**, 4, 26.

4. L. Schuerman. RTS,S malaria vaccine could provide major public health benefits. *The Lancet* **2019**, 394, 735-36.

5. P.G. Mathenge, S.K. Low, N.L. Vuong, M.Y.F. Mohamed, H.A. Faraj, G.I. Alieldin, R. Al Khudari, N.A. Yahia*et. al.* Efficacy and resistance of different artemisinin-based combination therapies: a systematic review and network meta-analysis. *Parasitol. Int.* **2020**, 74, 101919.

6. W. Pongtavornpinyo, I.M. Hastings, A. Dondorp, L.J. White, R.J. Maude, S. Saralamba, N.P. Day, N.J. White, M.F. Boni. ORIGINAL ARTICLE: Probability of emergence of antimalarial resistance in different stages of the parasite life cycle. *Evol. Appl.* **2009**, 2, 52.

7. J. Naß, T. Efferth. Development of artemisinin resistance in malaria therapy. *Pharm. Res.* **2019**, 146, 104275.

8. A.M. Thu, A.P. Phyo, J. Landier, D.M. Parker, F.H. Nosten. Combating multidrug-resistant*Plasmodium falciparum*malaria. *FEBS J.* **2017**, 284, 2569.

9. E.A. Ashley, A.P. Phyo. Drugs in development for malaria. *Drugs* **2018**, 78, 861.

10. G.M. Bwire, B. Ngasala, W.P. Mikomangwa, M. Kilonzi, A.A.R. Kamuhabwa. Detection of mutations associated with artemisinin resistance at k13-propeller gene and a near complete return of chloroquine susceptible falciparum malaria in southeast of Tanzania. *Sci. Rep.* **2020**, 10, 3500.

11. F.A. Siddiqui, R. Boonhok, M. Cabrera, H.G.N. Mbenda, M. Wang, H. Min, X. Liang, J. Qin*et. al.* Role of Plasmodium falciparum kelch 13 protein mutations in P. falciparum populations from northeastern Myanmar in mediating artemisinin resistance. *mBio* **2020**, 11, e01134.

12. K. Witmer, F.A. Dahalan, M.J. Delves, S. Yahiya, O.J. Watson, U. Straschil, D. Chiwcharoen, B. Sornboon*et. al.* Transmission of artemisinin-resistant malaria parasites to mosquitoes under antimalarial drug pressure. *Antimicrob. Agents Chemother.* **2020**, 65, e00898.

13. P. Liu In Natural Remedies in the Fight Against Parasites, H. F. Khater, M. Govindarajan, G. Benelli, Eds.; Intech: Ezypt, **2017**, pp 183-218.

14. P.P. Sharma, S. Kumar, K. Kaushik, A. Singh, I.K. Singh, M. Grishina, K.C. Pandey, P. Singh*et. al.* In silico validation of novel inhibitors of malarial aspartyl protease, plasmepsin V and antimalarial efficacy prediction. *J. Biomol. Struct. Dyn.* **2021**, 1-13.

15. S.K. Panda, S. Saxena, P.S.S. Gupta, M.K. Rana. Inhibitors of Plasmepsin X Plasmodium falciparum: Structure-based pharmacophore generation and molecular dynamics simulation. *J. Mol. Liq.* **2021**, 340, 116851.

16. C.-L. Ciana, R. Siegrist, H. Aissaoui, L. Marx, S. Racine, S. Meyer, C. Binkert, R. de Kanter*et. al.* Novel in vivo active anti-malarials based on a hydroxy-ethyl-amine scaffold. *Bioorganic Med. Chem. Lett.* **2013**, 23, 658-62.

17. P. Pino, R. Caldelari, B. Mukherjee, J. Vahokoski, N. Klages, B. Maco, C.R. Collins, M.J. Blackman*et. al.* A multistage antimalarial

18. P.M. Cheuka, G. Dziwornu, J. Okombo, K. Chibale. Plasmepsin Inhibitors in Antimalarial Drug Discovery: Medicinal Chemistry and Target Validation (2000 to Present). *J. Med. Chem.* **2020**, 63, 4445–67.

19. V. Hooda, P.B. Gundala, P. Chinthala. Sequence analysis and homology modeling of peroxidase from Medicago sativa. *Bioinformation* **2012**, 8, 974-79.

20. R.A. Friesner, R.B. Murphy, M.P. Repasky, L.L. Frye, J.R. Greenwood, T.A. Halgren, P.C. Sanschagrin, D.T. Mainz. Extra Precision Glide: Docking and Scoring Incorporating a Model of Hydrophobic Enclosure for Protein−Ligand Complexes. *Journal of Medicinal Chemistry* **2006**, 49, 6177-96.

21. T. Schwede, J. Kopp, N. Guex, M.C. Peitsch. SWISS-MODEL: An automated protein homology-modeling server. *Nucleic acids research* **2003**, 31, 3381-5.

22. R.A. Laskowski, M.W. MacArthur, D.S. Moss, J.M. Thornton. PROCHECK: a program to check the stereochemical quality of protein structures. *J. Appl. Cryst.* **1993**, 26, 283-91.

23. C. Colovos, T.O. Yeates. Verification of protein structures: patterns of nonbonded atomic interactions. *Protein science : a publication of the Protein Society* **1993**, 2, 1511-9.

24. D. Eisenberg, R. Lüthy, J.U. Bowie In Meth. Enzymol.; Academic Press: **1997**; Vol. 277, pp 396-404.

25. M. Wiederstein, M.J. Sippl. ProSA-web: interactive web service for the recognition of errors in three-dimensional structures of proteins. *Nucleic Acids Res.* **2007**, 35, W407-10.

26. S. Schrödinger Release 2020-1: Protein Preparation Wizard; Epik, LLC, New York, NY, 2020; Impact, Schrödinger, LLC, New York, NY; Prime, Schrödinger, LLC, New York, NY, 2020.

27. W. Tian, C. Chen, X. Lei, J. Zhao, J. Liang. CASTp 3.0: computed atlas of surface topography of proteins. *Nucleic acids research* **2018**, 46, W363-W67.

28. https://pubchem.ncbi.nlm.nih.gov/compound/5478883 (Accessed on July 15.

29. Schrödinger Release 2020-1: Maestro, Schrödinger, LLC, New York, NY, 2020.

30. S. Kumar, C. Upadhyay, M. Bansal, M. Grishina, B.S. Chhikara, V. Potemkin, B. Rathi, Poonam. Experimental and Computational Studies of Microwave-Assisted, Facile Ring Opening of Epoxide with Less Reactive Aromatic Amines in Nitromethane. *ACS Omega* **2020**, 5, 18746-57.

31. K.E.B. Parkes, D.J. Bushnell, P.H. Crackett, S.J. Dunsdon, A.C. Freeman, M.P. Gunn, R.A. Hopkins, R.W. Lambert, J.A. Martin. Studies toward the Large-Scale Synthesis of the HIV Proteinase Inhibitor Ro 31-8959. *J. Org. Chem.* **1994**, 59, 3656-64.

32. M. Stefanidou, C. Herrera, N. Armanasco, R.J. Shattock. Saquinavir Inhibits Early Events Associated with Establishment of HIV-1 Infection: Potential Role for Protease Inhibitors in Prevention. *Antimicrob. Agents Chemother.* **2012**, 56, 4381-90.

33. Schrödinger Release 2020-1: LigPrep, Schrödinger, LLC, New York, NY, 2020.

34. Schrödinger Release 2020-1: Epik, Schrödinger, LLC, New York, NY, 2020.

35. Schrödinger Release 2020-1: Glide, Schrödinger, LLC, New York, NY, 2020.

36. Schrödinger Release 2020-1: Prime, Schrödinger, LLC, New York, NY, 2020.

37. K.J. Bowers, E. Chow, H. Xu, R.O. Dror, M.P. Eastwood, B.A. Gregersen, J.L. Klepeis, I. Kolossvary*et. al.* In *Proceedings of the 2006 ACM/IEEE conference on Supercomputing*; Association for Computing Machinery: Tampa, Florida, 2006, p 84–es.

38. Schrödinger Release 2020-1: Desmond Molecular Dynamics System, D. E. Shaw Research, New York, NY, 2020. Maestro-Desmond Interoperability Tools, Schrödinger, New York, NY, 2020.

39. W.L. Jorgensen, J. Tirado-Rives. The OPLS [optimized potentials for liquid simulations] potential functions for proteins, energy minimizations for crystals of cyclic peptides and crambin. *J. Am. Chem. Soc.* **1988**, 110, 1657-66.

40. W.L. Jorgensen, D.S. Maxwell, J. Tirado-Rives. Development and Testing of the OPLS All-Atom Force Field on Conformational Energetics and Properties of Organic Liquids. *J. Am. Chem. Soc.* **1996**, 118, 11225-36.

41. W.L. Jorgensen, J. Chandrasekhar, J.D. Madura, R.W. Impey, M.L. Klein. Comparison of simple potential functions for simulating liquid water. *J. Chem. Phys.* **1983**, 79, 926-35.

42. G.J. Martyna, D.J. Tobias, M.L. Klein. Constant pressure molecular dynamics algorithms. *J. Chem. Phys.* **1994**, 101, 4177-89.

43. S. Nosé. A unified formulation of the constant temperature molecular dynamics methods. *J. Chem. Phys.* **1984**, 81, 511-19.

44. O. Trott, A.J. Olson. AutoDock Vina: Improving the speed and accuracy of docking with a new scoring function, efficient optimization, and multithreading. *Journal of Computational Chemistry* **2010**, 31, 455-61.

45. G. Janson, C. Zhang, M.G. Prado, A. Paiardini. PyMod 2.0: improvements in protein sequence-structure analysis and homology modeling within PyMOL. *Bioinformatics* **2017**, 33, 444-46.

46. A. Daina, O. Michielin, V. Zoete. SwissADME: a free web tool to evaluate pharmacokinetics, drug-likeness and medicinal chemistry friendliness of small molecules. *Sci. Rep.* **2017**, 7, 42717.

47. S. Kumar, Y. Gupta, S.E. Zak, C. Upadhyay, N. Sharma, A.S. Herbert, R. Durvasula, V. Potemkin*et. al.* A novel compound active against SARS-CoV-2 targeting uridylate-specific endoribonuclease (NendoU/NSP15): in silico and in vitro investigations. *RSC Medicinal Chemistry* **2021**, 12, 1757-64.

48. S. Singh, V. Rajendran, J. He, A.K. Singh, A.O. Achieng, Vandana, A. Pant, A.S. Nasamu*et. al.* Fast-Acting Small Molecules Targeting Malarial Aspartyl Proteases, Plasmepsins, Inhibit Malaria Infection at Multiple Life Stages. *ACS Infectious Diseases* **2019**, 5, 184-98.

49. N. Sharma, M. Kashif, V. Singh, D. Fontinha, B. Mukherjee, D. Kumar, S. Singh, M. Prudencio*et. al.* Novel Antiplasmodial Compounds Leveraged with Multistage Potency against the Parasite Plasmodium falciparum: In Vitro and In Vivo Evaluations and Pharmacokinetic Studies. *Journal of Medicinal Chemistry* **2021**, 64, 8666-83.

50. A.K. Singh, S. Rathore, Y. Tang, N.E. Goldfarb, B.M. Dunn, V. Rajendran, P.C. Ghosh, N. Singh*et. al.* Hydroxyethylamine Based Phthalimides as New Class of Plasmepsin Hits: Design, Synthesis and Antimalarial Evaluation. *PloS one* **2015**, 10, e0139347.

51. C. Upadhyay, N. Sharma, S. Kumar, P.P. Sharma, D. Fontinha, B.S. Chhikara, B. Mukherjee, D. Kumar*et. al.* Synthesis of the new analogs of morpholine and their antiplasmodial evaluation against the human malaria parasite Plasmodium falciparum. *New Journal of Chemistry* **2022**, 46, 250-62.

52. M. Smilkstein, N. Sriwilaijaroen, J.X. Kelly, P. Wilairat, M. Riscoe. Simple and inexpensive fluorescence-based technique for high-throughput antimalarial drug screening. *Antimicrobial agents and chemotherapy* **2004**, 48, 1803-6.